# Near ultraviolet photodissociation spectroscopy of $Mn^+(H_2O)$ and $Mn^+(D_2O)$

Wright L. Pearson III,[a] Christopher Copeland, Abdulkadir Kocak, Zachary Sallese, and Ricardo B. Metz[b]
*Department of Chemistry, University of Massachusetts Amherst, Amherst, Massachusetts 01003, USA*

(Received 1 October 2014; accepted 5 November 2014; published online 24 November 2014)

The electronic spectra of $Mn^+(H_2O)$ and $Mn^+(D_2O)$ have been measured from 30 000 to 35 000 $cm^{-1}$ using photodissociation spectroscopy. Transitions are observed from the $^7A_1$ ground state in which the $Mn^+$ is in a $3d^5 4s^1$ electronic configuration, to the $^7B_2$ ($3d^5 4p_y$) and $^7B_1$ ($3d^5 4p_x$) excited states with $T_0 = 30\,210$ and 32 274 $cm^{-1}$, respectively. Each electronic transition has partially resolved rotational and extensive vibrational structure with an extended progression in the metal−ligand stretch at a frequency of ∼450 $cm^{-1}$. There are also progressions in the in-plane bend in the $^7B_2$ state, due to vibronic coupling, and the out-of-plane bend in the $^7B_1$ state, where the calculation illustrates that this state is slightly non-planar. Electronic structure computations at the CCSD(T)/aug-cc-pVTZ and TD-DFT B3LYP/6-311++G(3df,3pd) level are also used to characterize the ground and excited states, respectively. These calculations predict a ground state Mn-O bond length of 2.18 Å. Analysis of the experimentally observed vibrational intensities reveals that this bond length decreases by 0.15 ± 0.015 Å and 0.14 ± 0.01 Å in the excited states. The behavior is accounted for by the less repulsive $p_x$ and $p_y$ orbitals causing the $Mn^+$ to interact more strongly with water in the excited states than the ground state. The result is a decrease in the Mn-O bond length, along with an increase in the H-O-H angle. The spectra have well resolved K rotational structure. Fitting this structure gives spin-rotation constants $\varepsilon_{aa}'' = -3 \pm 1$ $cm^{-1}$ for the ground state and $\varepsilon_{aa}' = 0.5 \pm 0.5$ $cm^{-1}$ and $\epsilon_{aa}' = -4.2 \pm 0.7$ $cm^{-1}$ for the first and second excited states, respectively, and $A' = 12.8 \pm 0.7$ $cm^{-1}$ for the first excited state. Vibrationally mediated photodissociation studies determine the O-H antisymmetric stretching frequency in the ground electronic state to be 3658 $cm^{-1}$. © *2014 AIP Publishing LLC*. [http://dx.doi.org/10.1063/1.4901982]

## I. INTRODUCTION

The importance of metal-water interactions in solvation, catalysis and biology has helped promote the study of metal-water complexes.[1] Due to the complexity of solution phase chemistry, the study of the intrinsic interaction between the metal and water is simplified by gas phase analysis. In particular, gas phase electronic spectroscopy experiments reveal information about a metal's electronic configuration and its effects on the ion's overall metal-water structure, including the metal-water bond.

Magnera, David, and Michl[2] and Marinelli and Squires[3] first measured the binding energies of gaseous water molecules to first-row transition metal cations using collision induced dissociation (CID) in a triple-quadrupole mass spectrometer. Magnera *et al.* have determined the $Mn^+$-$H_2O$ binding energy to be 11 400 $cm^{-1}$, while Marinelli and Squires have found it to be 12 900 $cm^{-1}$. These systems have been revisited in a guided-ion beam (GIB) measurement by Dalleska, Honma, Sunderlin, and Armentrout, who have obtained a binding energy of 9900 ± 500 $cm^{-1}$, making $Mn^+(H_2O)$ the most weakly bound first-row transition metal water complex.[4] In fact, along the periodic table from left to right the binding energies of the first-row transition metals to water follow a slight downward trend from $Ti^+$ to a minimum at $Mn^+$, before trending upward to $Ni^+$ and decreasing slightly to $Cu^+$. This is primarily because the $3d^5 4s^1$ ground state of $Mn^+(H_2O)$ leads to a less strongly bound complex than metals without electrons in the 4*s* orbital. Excitation of the $Mn^+(H_2O)$ $4p \leftarrow 4s$ transition results in strongly bound $3d^5 4p^1$ excited states. This differs from most $M^+(H_2O)$ complexes, whose low lying excited states are formed by $4s \leftarrow 3d$ transitions, where the excited states are more weakly bound than the ground state. Due to the large differences between the 4*s* and 4*p* orbital energies, the excited states of $Mn^+(H_2O)$ are well above the dissociation energy, resulting in the clean observation of the transitions by photodissociation spectroscopy.

Electronic spectroscopy of $M^+(H_2O)$ facilitates the measurement of ground and excited state bond dissociation energies and rotational constants, and excited electronic states vibrational frequencies. This information is used to determine the ground and excited electronic states geometries, bonding characteristics, etc. There have been many spectroscopic studies of $M^+(H_2O)$ complexes including electronic spectroscopy of hydrated alkaline earth cations $Mg^+(H_2O)$,[5] $Ca^+(H_2O)$,[6,7] $Sr^+(H_2O)$,[8] and transition metal cations $V^+(H_2O)$,[9,10] $Ni^+(H_2O)$,[11] $Co^+(H_2O)$,[12] and $Zn^+(H_2O)$.[13] Vibrational spectra of $M^+(H_2O)$ reveals information about the metal ion's effect on O-H bonds in the $H_2O$ ligand and can elucidate hydrogen-bonding networks in larger

[a] Present address: Department of Physics, J. R. Macdonald Laboratory, Kansas State University, Manhattan, Kansas 66506, USA.
[b] Author to whom correspondence should be addressed. Electronic mail: rbmetz@chem.umass.edu

 

water clusters. Duncan and co-workers have used argon tagging to measure vibrational spectra of $M^+(H_2O)_n$ (n = 1–4) (M = Sc,[14] V,[15] Cr,[16] Mn,[17] Fe,[18] Ni,[19] Cu,[20] Zn[21]) and $M^{2+}(H_2O)$ (M = Sc,[14] V,[22] Cr,[16] Mn[17]) in the O−H stretching region. Likewise, Nishi and co-workers measured vibrational spectra of $M^+(H_2O)_n$ for M = V,[23] Co,[24] Cu and Ag,[25] while Zhou and co-workers measured the vibrational spectra of $Au^+(H_2O)_n$ (n = 1–8).[26] In addition, van der Linde and Beyer have examined water activation in larger clusters of $M^+(H_2O)_n$ (n < 40) (M = V, Cr, Mn, Fe, Co, Ni, Cu, Zn) in a FT-ICR mass spectrometer, with particular emphasis on water activation in $Mn^+(H_2O)_n$.[27] O′Brien and Williams used vibrational spectroscopy to observe similar effects in smaller divalent clusters (n = 5–8).[28] Rosi and Bauschlicher have investigated binding energies of $M^+(H_2O)_n$ (n = 1–4) for transition metals from V to Zn.[29] They calculate the structure of $Mn^+(H_2O)$ to be planar, with $C_{2v}$ symmetry and note that due to the absence of 3*d*-4*s* hybridization, metal-water repulsion is reduced by polarization of the 4*s* orbital away from the water by 4*s*-4*p* hybridization. This structure has been confirmed in subsequent calculations by Trachtman *et al.*[30] and Irigorias *et al.*[31] who also noted that the septet $Mn^+$ ion is not likely to accept donations from the water due to the $Mn^+$ ion's highly stabilized exchange energy due to its six matching spins. Calculations by Carnegie *et al.* in support of the vibrational spectra of $Mn^+(H_2O)$ predict a binding energy of 10 600 $cm^{-1}$.[17]

As previously mentioned, the vibrational spectra of $Mn^+(H_2O)$ and $Mn^{2+}(H_2O)$ have been measured by Duncan and coworkers via argon tagging.[17] Although the attached argon typically only slightly perturbs the O-H stretching frequencies, it strongly affects the rotational constants. Our group used photodissociation spectroscopy and vibrationally mediated photodissociation (VMP) to measure the electronic spectra and O−H stretching frequencies of untagged $Ni^+(H_2O)$ and $Co^+(H_2O)$.[11,12] Those studies also measured the rotational constants $\varepsilon$ and A for the ground and excited electronic states. The current experiments extend the electronic and vibrational spectroscopy studies to the $Mn^+(H_2O)$ and $Mn^+(D_2O)$ complexes.

## II. EXPERIMENTAL METHODS

The experiments are carried out on a laser ablation dual time-of-flight reflectron mass spectrometer described in earlier papers.[32,33] Manganese ions are produced by ablating a manganese rod with the 532 nm second harmonic of a pulsed Nd:YAG laser operating at 17 mJ/ pulse at a repetition rate of 20 Hz. A gas mix of 2%–10% $H_2$ and 90%–98% He at a pressure of 35 psi runs through a bubbler filled with purified $H_2O$ or $D_2O$. The resulting mixture is introduced through a piezoelectric pulsed valve into the chamber where the $Mn^+$ ions interact with the gas to form $Mn^+(H_2O)$ and larger clusters. The ions then expand into vacuum forming a beam with a rotational temperature of ∼15 K.[12] The ion beam passes through a skimmer into the time-of-flight mass spectrometer, where the ions are accelerated, re-referenced to ground potential and mass selected. At the turning point of the reflectron, the frequency-doubled output of a tunable dye laser is used to photodissociate the ions. The fragment and remaining parent ions are reaccelerated and strike a microchannel plate detector in the final stage of the time-of-flight mass spectrometer. The signal is amplified and collected on an oscilloscope and gated integrators (controlled by an inhouse *LabView* program for data acquisition) and mass analyzed. A photodissociation spectrum is formed by plotting the ratio of $Mn^+$ fragment ions to $Mn^+(H_2O)$ or $Mn^+(D_2O)$ parent ions, normalized to laser power, as a function of the wavelength.

Although loss of $H_2O$ is expected and observed to be the primary photodissociation pathway, loss of H atom and $H_2$ are energetically accessible above 23 800 and 27 400 $cm^{-1}$, respectively. Difference (laser on - laser off) mass spectra of $Mn^+(H_2O)$ taken at several wavelengths show that H atom loss is ≤20% of $H_2O$ loss while no $H_2$ loss is detected. Loss of D from $Mn^+(D_2O)$ is even smaller, <5% of $D_2O$ loss. Photodissociation spectra are obtained by monitoring loss of water ($Mn^+$), as the other channels are too small and too close to the parent.

The electronic spectroscopy studies utilize the frequency-doubled output of a Continuum ND6000 dye laser at a line width of 0.1 $cm^{-1}$ using a variety of laser dyes to scan the 270–360 nm range. The photodissociation yield is linear with laser power, up to ∼2–3 mJ/pulse. As a result, the unfocused UV laser beam is attenuated to <3 mJ/pulse to reduce power broadening and faithfully reproduce spectral intensities. The dye laser wavelength is calibrated using the optogalvanic spectrum of neon.[34] The infrared spectroscopy experiments employ a Laser Vision IR OPO/OPA tunable from 2200 $cm^{-1}$ to >4000 $cm^{-1}$. This laser produces 10 mJ/pulse at ∼3500 $cm^{-1}$, with a line width of ∼2 $cm^{-1}$. It is calibrated using the absorption spectrum of water vapor. A multipass mirror arrangement allows the IR laser to make up to 11 passes through the ion cloud. However, the UV beam only makes one pass through the ion cloud due to absorption by the mirrors.[35] The computations use the *Gaussian 09* suite of programs.[36] The geometries, energies, and vibrational frequencies of the ground and excited states of $Mn^+(H_2O)$ and $Mn^+(D_2O)$ are calculated with the B3LYP hybrid density functional with the 6-311++G(3df,3pd) basis set. The ground state geometry is also calculated at the CCSD(T)/aug-cc-pVTZ level.

## III. RESULTS AND DISCUSSION

### A. Electronic spectroscopy

Photodissociation spectra of $Mn^+(H_2O)$ and $Mn^+(D_2O)$ are measured from 30 000 to 35 000 $cm^{-1}$ as shown in Figure 1. A full scan of 27 000–38 000 $cm^{-1}$ revealed no additional dissociation. The photodissociation spectrum has transitions to two excited electronic states, each with well-structured vibrational features. In addition, the spectrum of $Mn^+(H_2O)$ shows partially resolved rotational structure.

To assign the spectra the possible motions of the complex are first considered. The $Mn^+(H_2O)$ ion has six vibrations, three of which essentially belong to $H_2O$; the symmetric and antisymmetric O-H stretches and the H-O-H bend. There are also three low frequency vibrations: the $Mn^+$-$H_2O$ stretch and two $Mn^+$-$H_2O$ bends. The vibrational modes and their quantum numbers are assigned with the aid of the spectrum of the

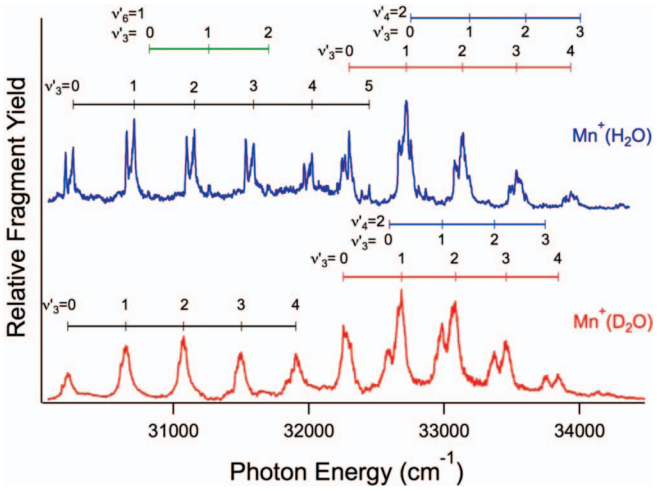


FIG. 1. Photodissociation spectra of $Mn^+(H_2O)$ and $Mn^+(D_2O)$ from 30 000 to 35 000 $cm^{-1}$. An extended progression is observed in the Mn-ligand stretch ($\nu_3'$), in conjunction with short progressions in the in-plane bend ($\nu_6'$) and out-of-plane bend ($\nu_4'$).

deuterated ion. Deuteration should significantly alter the frequency of the water stretches and bend, and of the intermolecular bends, but have little effect on the metal-ligand stretching frequency, as this vibration primarily involves heavy atom motion. The primary vibrational progression shows very similar frequencies of ~460 $cm^{-1}$ in $Mn^+(H_2O)$ and ~440 $cm^{-1}$ in $Mn^+(D_2O)$. This confirms that the primary vibration observed is due to the metal-water stretch ($\nu_3$).

Isotopic substitution also confirms the assignment of the band origins for the two excited electronic states: at ~30 250 $cm^{-1}$ and ~32 300 $cm^{-1}$, respectively. These excited state progressions are due to $Mn^+(H_2O)$ with the metal in its $3d^5 4p^1$ state. The manganese ion's interaction with $H_2O$ splits the degeneracy of the 4*p* orbital into three components: $p_x$, $p_y$, and $p_z$. Figure 2 shows the molecular axis system and Figure S1 in the supplementary material shows the relevant molecular orbitals.[45] One would expect the electronic spectrum of $Mn^+(H_2O)$ to consist of three bands, transitions to the nearly degenerate $p_x$ and $p_y$, along with a transition to the $p_z$ orbital at significantly higher energy. This is supported by TD-DFT calculations, which predict vertical excitation energies of 32 600 $cm^{-1}$ to the $^7B_2$ ($p_y$) state, 34 330 $cm^{-1}$ to the $^7B_1$ ($p_x$) state, and 38 360 $cm^{-1}$ to the $^7A_1$ ($p_z$) state. The $p_y$ orbital is the least repulsive of the three. Thus the lowest energy band is due to a transition from the $^7A_1$ ($3d^5 4s$) ground state to the $^7B_2$ ($3d^5 4p_y$) excited state. The $p_x$ is slightly more repulsive as it overlaps the lone pair orbital on the oxygen. This transition ($^7B_1$ ($3d^5 4p_x$) ← $^7A_1$ ($3d^5 4s$)) is responsible for the second band. Finally, the $p_z$ orbital is the most repulsive as it points directly at the ligand. Therefore it is expected that the transition will have the highest energy. However, this transition is not observed, owing to either being at a higher energy than 38 000 $cm^{-1}$ or a large change in geometry leading to very broad spectra. Although similar $p_x$,$p_y$ ← s transitions have been observed in $Mg^+(H_2O)$, $Ca^+(H_2O)$ and $Zn^+(H_2O)$, the $p_z$ ← s has not.[6,13,37]

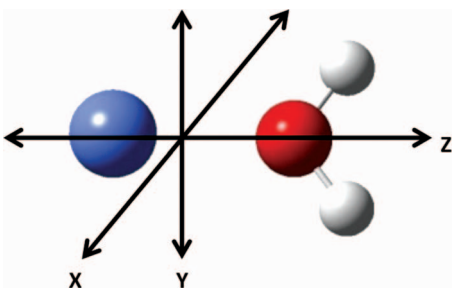


FIG. 2. Rotational axis diagram of $Mn^+(H_2O)$.

In the spectra there are also short progressions in two other intermolecular vibrations. Their assignment is facilitated by considering the rotational structure. The electronic transition moment from the 4*s* to the $4p_x$ and $4p_y$ orbitals lies perpendicular to the Mn-O axis. Being a near prolate symmetric top, $Mn^+(H_2O)$ has a very small moment of inertia for rotation about the Mn-O axis. Hence the *B* and *C* constants are nearly equal and much smaller (~0.25 $cm^{-1}$) than the relatively large rotational constant $A \approx 14$ $cm^{-1}$. As a result, transitions to final states that have $A_1$ vibrational symmetry should show perpendicular rotational structure, creating multiplets with $\Delta K_a = \pm 1$. At the ~15 K temperature of the ion beam, three main peaks in the rotational substructure are expected, corresponding to $K_a' = 1 \leftarrow K_a'' = 0$ and $K_a' = 0$, $2 \leftarrow K_a'' = 1$. This is observed for the metal-ligand stretch progression. Small singlet features associated with parallel rotational structure ($\Delta K_a = 0$) are also observed in the $^7B_2$ state starting at 30 816 $cm^{-1}$. These peaks are the result of the in-plane bend ($\nu_6$) alone and in combination with the $M^+$-$H_2O$ stretch The out-of-plane bend ($\nu_4$) is seen in the $^7B_1$ state of both $Mn^+(H_2O)$ and $Mn^+(D_2O)$ starting at 32 753 and 32 591 $cm^{-1}$, respectively, and also in combination with the $M^+$-$H_2O$ stretch. Each of the three observed vibrations will be analyzed in turn.

To better characterize the metal-ligand stretching interaction, the peak positions are fit to the energy levels of a Morse oscillator (Eq. (1)).

$$E = T_e + \omega_3'(v_3' + 1/2) - \chi_3'(v_3' + 1/2)^2. \quad (1)$$

Here, $\omega_3'$ is the fundamental frequency, $v_3'$ is the vibrational quantum number, and $\chi_3'$ is the anharmonicity constant. First and second excited state frequencies of $\omega_3'$ = 459 $cm^{-1}$ and 430 $cm^{-1}$ are determined with anharmonicities of $\chi_3' = 3.5$ $cm^{-1}$ and 4.1 $cm^{-1}$, respectively. The ground and excited state values are also obtained at the B3LYP/6-311++G(3df,3pd)) level. Table I summarizes these vibrational frequencies for $Mn^+(H_2O)$ and $Mn^+(D_2O)$.

To further complete the picture, the binding energies of $Mn^+(H_2O)$ excited states are also calculated. The ground state of $Mn^+$ is $3d^5 4s^1$ ($^7S_3$); the lowest allowed electronic transition is $4p \leftarrow 4s$ which produces the $^7P_{2,3,4}$ states at 38 366, 38 543, and 38 806 $cm^{-1}$, respectively.[38] Using this information, the experimentally determined dissociation energy of the $Mn^+(H_2O)$ ground state $D_0 = 9900 \pm 500$ $cm^{-1}$,[4] and the observed $p_x$ and $p_y$ band origins, the binding energies of the excited states are determined. These values are 18 200 ± 500 $cm^{-1}$ for the $^7B_2(p_y)$ and 16 200 ± 500 $cm^{-1}$ for the

TABLE I. Calculated and measured vibrational frequencies ($cm^{-1}$) of $Mn^+(H_2O)$ and $Mn^+(D_2O)$.

| Mode ($\nu_i$) | Vibrational symmetry | Description | $Mn^+(H_2O)$ Ground state | $^7B_2$ | $^7B_1$ | $Mn^+(D_2O)$ Ground state | $^7B_2$ | $^7B_1$ |
|---|---|---|---|---|---|---|---|---|
| | | | Calculated (B3LYP/6-311++G(3df,3pd)) | | | | | |
| 1 | $a_1$ | O-H symmetric stretch | 3720 | 3744 | 3723 | 2680 | 2695 | 2684 |
| 2 | $a_1$ | H-O-H bend | 1644 | 1624 | 1650 | 1206 | 1193 | 1210 |
| 3 | $a_1$ | M-O stretch (z) | 310 | 463 | 427 | 297 | 443 | 411 |
| 4 | $b_1$ | Out-of-plane bend (x) | 320 (361) | 357 (257) | 280 (106)[a] | 245 (270) | 269 (183) | 213 (55)[b] |
| 5 | $b_2$ | O-H antisymmetric stretch | 3802 | 3799 | 3790 | 2789 | 2788 | 2779 |
| 6 | $b_2$ | In-plane bend (y) | 494 (493) | 548 (533) | 660 (584) | 366 (367) | 408 (398) | 487 (435) |
| | | | Experimental | | | | | |
| 3 | $a_1$ | M-O stretch (z) | ... | 459[c] | 430[d] | ... | 436 | 404 |
| 4 | $b_1$ | Out-of-plane bend (x) | ... | ... | 456[e] | ... | ... | 306[e] |
| 5 | $b_2$ | O-H antisymmetric stretch | 3658 | ... | ... | ... | ... | ... |
| 6 | $b_2$ | In-plane bend (y) | ... | 559 | ... | ... | ... | ... |

[a]This vibration is anharmonic, the value shown is the 0-1 spacing; the 0-2 spacing is 364 $cm^{-1}$.
[b]The value shown is the 0-1 spacing; the 0-2 spacing is 240 $cm^{-1}$. Values in parentheses are $\nu_0$ and are obtained by numerically solving the 1D Schrodinger equation, for a scan along this coordinate.
[c]$\chi'_3 = 3.5$.
[d]$\chi'_3 = 4.1$.
[e]v = 0-2 spacing.

$^7B_1(p_x)$ states, which are significantly higher than the binding energies in the ground state. In comparison, calculating $D_0$ purely based on the measured $Mn^+$-$H_2O$ stretching frequency and anharmonicity utilizing Birge-Sponer plots gives ~15 000 and 11 000 $cm^{-1}$ for the $^7B_1$ and $^7B_2$ states, respectively. This is somewhat lower than the values derived from the ground state dissociation energy. The discrepancy is due to being limited to the observed spectra's modest number of vibrational levels, which only encompass the first 15% of the dissociation energy. In their study of the electronic spectrum of $Co^+$(Ne) Mosley *et al.* demonstrate that the binding energy extrapolated using Birge-Sponer plots gives different values depending the range of vibrational states used in the fit.[39]

The relative intensities of the vibrational features in the photodissociation spectrum reflect the change in geometry upon electronic excitation. In order to quantify this, the one dimensional Schrödinger equation for the Mn-($H_2O$) stretch is solved. Treating the ground and excited electronic states as Morse oscillators, the vibrational (Franck-Condon) overlaps are calculated while varying the upper state Mn-O bond length. For the ground state, these calculations use the B3LYP/6-311++G(3df,3pd) bond length of 2.180 Å, $Mn^+$-O stretching frequency of 309.7 $cm^{-1}$ and experimental dissociation energy. For the excited states, experimental frequencies and anharmonicities are used and the bond length is varied until the calculated intensities match the experiment. The bond lengths are $r_e = 2.030 \pm 0.015$ Å and $2.040 \pm 0.01$ Å for the first and second excited states, respectively. The p←s excitation leads to a reduction in the Mn-O bond length of ~0.15 Å. This is slightly larger than the ~0.13 Å shortening observed for the analogous transition in $Zn^+(H_2O)$ and 0.09 Å in $Ca^+(H_2O)$.[6,13] The bond length decrease is due to repulsion between the electron in the singly occupied 4*s* orbital and the lone pairs on the oxygen. Promotion of this electron to the $4p_x$ or $4p_y$ orbital, both of which are perpendicular to the ligand, reduces this repulsion and leads to a shorter, stronger $Mn^+$-$H_2O$ bond. Morse potential curves for the ground and excited states observed are shown in Figure 3. As shown in Table I, the calculated TDDFT harmonic frequencies for the Mn-$H_2O$ stretch in the excited states are surprisingly close to the experimental frequencies, differing by <1%. In addition, the calculated Mn-O bond lengths are also in good accord with experiment (Table II).

The observed photodissociation yield is quite small, considering that each band has a calculated oscillator strength $f \approx 0.2$. There are several possible reasons for the low photofragment yield. Internal conversion to the ground state could be inefficient due to the large difference in energy between the $p_x$ and $p_y$ excited states and the ground state, as is intersystem crossing to states correlating to $Mn^+(^5S,^5D)$ + $H_2O$ due to small spin-orbit coupling. If this is the case, fluorescence might compete with photofragmentation. Another possible mechanism is that the initially excited molecules absorb a second photon prior to dissociating. In principle this would result in a quadratic power dependence, rather than the linear dependence observed. However, if the oscillator strength for the second transition is substantially

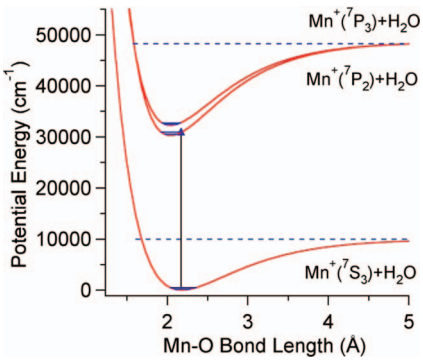


FIG. 3. Potential energy curves of the ground and excited electronic states of $Mn^+(H_2O)$ along the Mn−O stretch based on experiment.

TABLE II. Geometries of the ground and excited states of $Mn^+(H_2O)$.

| | Calculated, B3LYP/6-311++G(3df,3pd) or CCSD(T)/aug-cc-pVTZ | | | Experiment |
|---|---|---|---|---|
| $Mn^+(H_2O)$ | $r_{MO}$ (Å) | ∠HOH (deg) | $r_{OH}$ (Å) | $r_{MO}$ (Å) |
| Ground state | 2.180 | 106.8 | 0.968 | ... |
| Ground state[a] | 2.177 | 106.1 | 0.967 | ... |
| Excited state $1(4p_y)^7B_2$ | 2.001 | 109.6 | 0.967 | 2.030 ± 0.015 |
| Excited state $2(4p_x)^7B_1$ | 2.040 | 107.0 | 0.969 | 2.040 ± 0.010 |

[a]At the CCSD(T)/aug-cc-pVTZ level.

lower than the first, the quadratic regime would occur at low laser powers where the dissociation could not be accurately monitored. Scurlock *et al.* discuss these possibilities in detail for $Ca^+(H_2O)$.[6]

As previously mentioned, the in-plane bend ($\nu_6'$) is observed for $Mn^+(H_2O)$ in the first excited state and the out-of-plane bend ($\nu_4'$) for $Mn^+(H_2O)$ and $Mn^+(D_2O)$ in the second excited state. The in-plane bend is seen as a result of vibronic coupling, while the out-of-plane bend results from a geometry change along that mode. A consequence of vibronic coupling is that only one quantum of in-plane bend is observed, whereas only transitions to even quanta are seen for the out-of-plane bend.

The in-plane bend ($\nu_6'$) is observed in the first excited state, starting 559 $cm^{-1}$ after the origin, and then in combination with the metal-ligand stretch. This result is very close to the calculated harmonic frequency of 548 $cm^{-1}$. Both the in-plane bend and $p_y$ orbital have $B_2$ symmetry. Their symmetry product, $A_1$, indicates a vibronically allowed transition and appears as a parallel band. The analogous, vibronically allowed transition is also observed in $Zn^+(H_2O)$, at 700 $cm^{-1}$.[13] In $Mn^+(D_2O)$ the in-plane bend is predicted to lie at 408 $cm^{-1}$. It is thus obscured by the much more intense metal-ligand stretch at 436 $cm^{-1}$.

Transitions to two quanta of the out-of-plane bend ($\nu_4'$) are seen in the second excited state of both $Mn^+(H_2O)$ and $Mn^+(D_2O)$. Transitions to even number of quanta in $\nu_4'$ show perpendicular rotational structure. These peaks are clearly observed in $Mn^+(D_2O)$ and give $2\nu_4' = 306$ $cm^{-1}$. In the $Mn^+(H_2O)$ spectrum, $2\nu_4' = 456$ $cm^{-1}$ is only ~26 $cm^{-1}$ larger than $\nu_3'$. As a result, the multiplet structure of transitions to states with $\nu_4' = 2$ and $\nu_3' = n$ overlap multiplets with $\nu_4' = 0$ and $\nu_3' = n+1$, convoluting the spectrum. Transitions to one quantum of $\nu_4'$ are vibronically allowed for the second excited state and would show parallel structure, but they are not observed in this case, although they are seen in $Zn^+(H_2O)$ and $Ca^+(H_2O)$.[6,13] Time-dependent DFT calculations are carried out to further characterize the out-of-plane bend in the ground and excited electronic states of $Mn^+(H_2O)$. The potentials are calculated by scanning the out-of-plane angle from 0° to 90° (keeping the Mn-O bond length and H-O-H angle fixed at the equilibrium value in the ground state) and then using TDDFT to find the total energy at that geometry. As shown in Figure 4, the out-of-plane bend is harmonic for the ground state, but the second excited state has

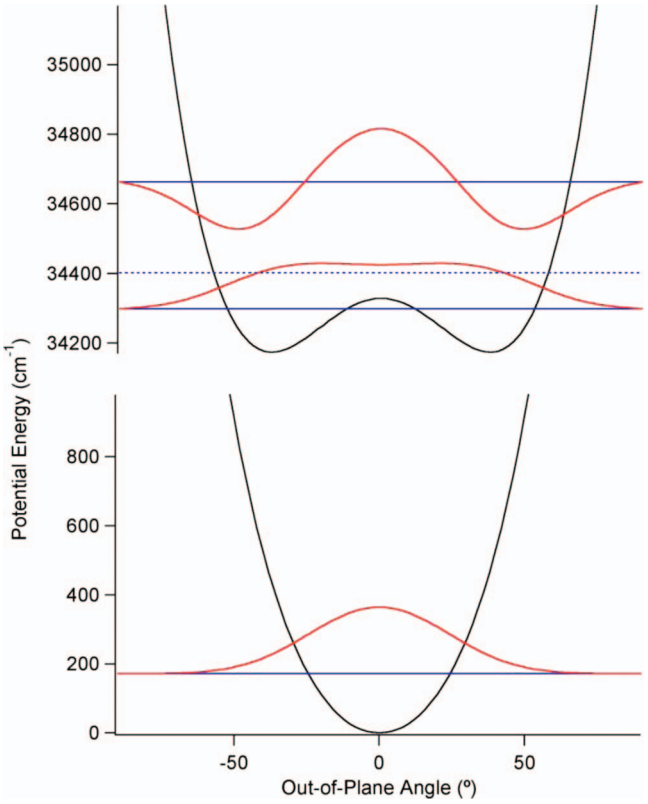


FIG. 4. Scans along the out-of-plane bend mode in the ground and $^7B_1$ excited state showing the vibrational energy levels for $\nu_3'' = 0$ and $\nu_3' = 0$, 1, and 2 and the corresponding wavefunctions for states with even quanta.

two equivalent minima at ±38°, separated by a barrier of 154 $cm^{-1}$. Energies and wavefunctions of the excited states are calculated by solving the one dimensional Schrödinger equation. For the second excited state of $Mn^+(H_2O)$ $\nu_3' = 1$ is predicted to lie 106 $cm^{-1}$ above $\nu_3' = 0$, with $\nu_3' = 2$ at 364 $cm^{-1}$. This is slightly lower than the 456 $cm^{-1}$ observed experimentally. The calculated values for $Mn^+(D_2O)$ are similarly underestimated as seen in Table I. In addition, the Franck-Condon factors calculated for $\nu_3' = 2$ are smaller than is observed. This suggests that the TDDFT calculations underestimate the barrier to planarity.

The vibrational structure in the electronic spectra of $Mn^+(H_2O)$ reveals how the electron occupancy of the metal affects the bonding with the ligand. The $(3d^5 4s)$ ground state of $Mn^+$ binds to water relatively weakly, forming a planar, $C_{2v}$ complex with a calculated Mn-O bond length of 2.18 Å. The $3d^5 4p_y$ excited state has a much shorter bond length (2.03 Å) and a metal-ligand stretching frequency of 459 $cm^{-1}$, and retains the $C_{2v}$ structure. In the second, $3d^5 4p_x$, excited state the bond is slightly longer (2.04 Å), the metal-ligand stretching frequency drops slightly to 430 $cm^{-1}$ and the complex distorts out-of-plane. The electronic spectrum of $Mn^+(H_2O)$ is quite similar to that of $Zn^+(H_2O)$. Both have long progressions in the metal-water stretch which are indicative of significant changes in bond length from the ground to the excited state. In the first excited state they both also show a vibronically allowed transition to the in-plane bend and in the second excited state a short progression in the out-of-plane

bend, indicating a small barrier to planarity. The $Zn^+(H_2O)$ system does show stronger, shorter bonds in the ground and excited electronic states, as would be expected considering the smaller ionic radius of zinc. For example, the calculated Zn-$H_2O$ bond length of 2.07 Å in the ground state reduces to 1.95 Å and 1.98 Å in the excited states, and the vibrational frequencies of the excited states of $Zn^+(H_2O)$ are ∼15% higher than the corresponding states in $Mn^+(H_2O)$. In the second excited state, the $4p_x$ orbital on the metal overlaps the lone pair electrons on the oxygen. This is more repulsive than the interaction in the first excited state in which the $4p_y$ orbital is perpendicular to the oxygen lone pair. This repulsion leads to the $p_x$ state lying ∼2000 $cm^{-1}$ above the $p_y$ state and having a slightly longer bond. The energy difference between these two states is small; a consequence of the metal's 4*p* orbitals being much larger than the oxygen atom's lone pair orbitals.

### B. Electronic spectroscopy: Rotations

Analysis of the rotational structure in the electronic transitions potentially provides information about the geometry of the molecule and the symmetry of the ground and excited states. In this analysis $Mn^+(H_2O)$ and $Mn^+(D_2O)$ are treated as nearly symmetric prolate tops. The corresponding spectra's rotational structure are compared to simulations generated by the *spfit* and *spcat* programs[40] to determine A′, B′ (B′ ≈ C′) rotational and $\varepsilon_{aa}'$ and $\varepsilon_{aa}''$ spin-rotational constants.

The rotational Hamiltonian is expressed as the sum of purely rotational and spin-rotation terms:[41,42]

$$\boldsymbol{H} = \boldsymbol{H}_{rot} + \boldsymbol{H}_{sr} \tag{2}$$

with

$$\boldsymbol{H}_{rot} = A\boldsymbol{N}_a^2 + B\boldsymbol{N}_b^2 + C\boldsymbol{N}_c^2, \tag{3}$$

$$\boldsymbol{H}_{sr} = \frac{1}{2}\sum_{\substack{\alpha=a,b,c\\ \beta=a,b,c}} \varepsilon_{\alpha,\beta}\left(\boldsymbol{N}_\alpha S_\beta + S_\beta \boldsymbol{N}_\alpha\right), \tag{4}$$

where A, B, and C are rotational constants, **N** is the rotational angular momentum, S is the spin angular momentum, and $\varepsilon_{\alpha,\beta}$ are components of the spin rotation tensor in the inertial axis system (a, b, c). In the absence of spin-rotational interaction the rotational energies (eigenvalues for $H_{rot}$) for a near-symmetric top are given by Eq. (5).

$$E_{J,K_a} = \left(A - \left(\frac{B+C}{2}\right)\right)K_a^2 + \left(\frac{B+C}{2}\right)J(J+1). \tag{5}$$

The quantum numbers associated with rotations are the total angular momentum quantum number J, and $K_a$, the projection of the angular momentum onto the Mn-O bond (Figure 2). Rotation about the Mn-O bond has the smallest moment of inertia and hence the largest rotational constant. In the ground state, this is calculated as $A'' \approx 14$ $cm^{-1}$. The *B* and *C* constants are much smaller and are degenerate for a prolate top. They are nearly identical to each other, and in the ground state are calculated as $B'' \approx C'' \approx 0.24$ $cm^{-1}$. As noted earlier, the K structure is apparent in the spectrum but individual J peaks are not resolved. Although the spin-rotation interaction parameter $\varepsilon$ has components along all three rotational axes, $\varepsilon_{aa}$ dominates as the *A* rotational constant is much larger than *B* or *C*. The spin-rotation constant $\varepsilon_{aa}$ adds two primary terms to the energies in Eq. (5).[7,43] One term is proportional to $\varepsilon_{aa}K_a\Sigma$, ($\Sigma = -3, -2, -1, 0, 1, 2, 3$ is the projection of the electron spin angular momentum onto the *a* axis) which broadens peaks with $K_a \geq 1$ and the other to $\varepsilon_{aa}K_a^2$, which affects the apparent *A* rotational constant. The shape of each $K_a' \leftarrow K_a''$ peak is determined by the spin-rotation constants in the upper and lower states, and to a lesser extent, by the change in the *B* and *C* rotational constants ($\Delta B$, $\Delta C$) upon electronic excitation. This is reflected in the simulations that are much more sensitive to $\Delta B$ than to the individual values of $B'$ and $B''$.

Since hydrogen is a fermion, the overall wavefunction for $Mn^+(H_2O)$ must be antisymmetric with respect to exchange of the hydrogens (which is equivalent to 180° rotation about the *a* axis). The ground state of $Mn^+(H_2O)$ is $^7A_1$ (symmetric), as is the vibrational wavefunction for $v'' = 0$. So, the product of the wavefunction for rotation about the *a* axis and the nuclear spin must be antisymmetric, which results in a 1:3 even:odd $K_a''$ population ratio, if it is difficult to effectively cool molecules from $K_a'' = 1$ to $K_a'' = 0$ in the ion source.[12] Thus, the perpendicular bands in the spectrum of $Mn^+(H_2O)$ appear as doublets, due to the $K_a' = 0 \leftarrow K_a'' = 1$ and $K_a' = 2 \leftarrow K_a'' = 1$ transitions. The $K_a' = 1 \leftarrow K_a'' = 0$ transition lies between these features, but it is much less intense and, for most bands in $Mn^+(H_2O)$, does not give a discrete peak. States with $K_a'' > 1$ have very low population at 15 K and thus contribute little to the spectrum. As deuterium is a boson, $Mn^+(D_2O)$ should have a 2:1 even:odd $K_a''$ ratio.[12] The spectrum should thus consist primarily of triplets, with a central $K_a' = 1 \leftarrow K_a'' = 0$ peak bracketed by weaker $K_a' = 0, 2 \leftarrow K_a'' = 1$ peaks (which are bracketed in turn by much weaker $K_a' = 1, 3 \leftarrow K_a'' = 2$ peaks). Unfortunately, the rotational structure in $Mn^+(D_2O)$ is substantially broader than in $Mn^+(H_2O)$, so the K structure is barely observable. Due to the limited resolution of the spectrum, some spectroscopic parameters could not be determined.

Parameterization of the *spfit* and *spcat* program[40] begins with the determination of the equilibrium constants $A_e''$, $B_e''$, and $C_e''$, which are calculated at the CCSD(T)/aug-cc-pVTZ level. These values are then converted to $v = 0$ constants $A_0''$, $B_0''$, and $C_0''$ by adding the difference between equilibrium and $v = 0$ constants from an anharmonic frequency calculation at the B3LYP/6-311++G(3df,3pd) level. The rotational simulations are relatively insensitive to B and C, so these constants were set to the values obtained from the intensities in the Mn-O stretch progressions: $\Delta r_{M\text{-}O} = 0.15 \pm 0.015$ Å ($B' = 0.279 \pm 0.004$ $cm^{-1}$) and $0.14 \pm 0.01$ Å ($B' = 0.277 \pm 0.003$ $cm^{-1}$). Excited state terms $A'$, $B'$, $\varepsilon_{aa}'$, and ground state $\varepsilon_{aa}''$ are then varied until the generated spectrum best approximates the experiment. The temperature in the simulations is held at 15 K, as in the $Ni^+(H_2O)$ and $Co^+(H_2O)$ studies.[11,12] A Lorentzian line width of 2 $cm^{-1}$ is also used, to reflect the excited state lifetime. The results are seen in Figure 5 with corresponding rotational parameters in Table III.

Comparing the ground to excited states in Table III, the *A* constant decreases and the *B* and *C* constants increase

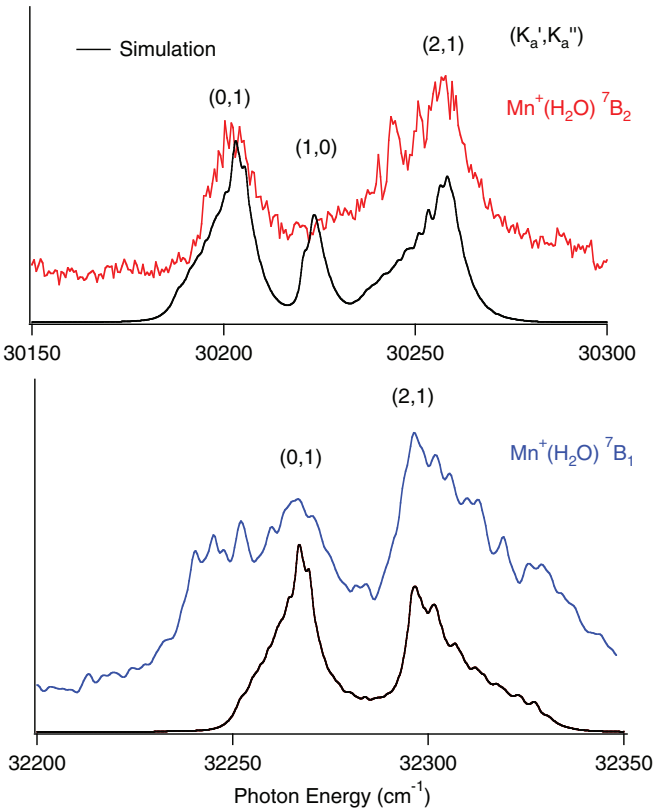


FIG. 5. Photodissociation spectra of the origin band of the $^7B_2$ state (top) and $^7B_1$ state of $Mn^+(H_2O)$ (bottom) showing the $\Delta K_a = \pm 1$ features characteristic of a perpendicular transition. The simulated spectra are also shown, using the spectroscopic parameters in Table III, a rotational temperature of 15 K, and a Lorentzian line width of 2 $cm^{-1}$.

during the transition. This increase in *B* and *C* is the result of the shortening of the Mn-O bond upon electronic excitation. For the planar complexes, the *A* constant depends on $r_{OH}$ and ∠HOH. As the calculations predict that electronic excitation has an insignificant effect on $r_{OH}$ (Table II), the change in *A* is thought largely due to a change in the H-O-H angle. The observed $A' = 12.8 \pm 0.7$ $cm^{-1}$ for the $^7B_2$ state corresponds to ∠HOH = 112° ± 4°. Fits of *A* and $\varepsilon_{aa}$ are correlated as their effect on the energies is proportional to $K_a^2$. Therefore, the relatively large uncertainty in *A* includes the effects caused by varying $\varepsilon_{aa}'$. In comparison, the ground state ∠HOH is calculated as 106.1° at the CCSD(T)/aug-cc-pVTZ level of theory. This increase in the ∠HOH for states with shorter metal ion-oxygen bonds has also been observed in $M^+(H_2O)$ (M = Mg, Ca, Co, Ni, Zn).[6,11–13,37] In bare $H_2O$, the ∠HOH is 104.5°. This is smaller than the tetrahedral angle (109.5°), due to repulsion between the O-H bonding electrons and the oxygen lone pairs. When a metal ion binds to water, it removes electron density from the oxygen lone pairs, which increases the ∠HOH. For a particular metal, this effect is stronger the shorter the M-O bond. For the $^7B_1$ state, the simulations do not reproduce the very broad $K_a' = 0 \leftarrow K_a'' = 1$ peak in the origin band, and peaks with $v_3' > 0$ overlap those with $v_4' = 2$, making *A*′ impossible to determine. Given that *A*′ should not differ to an appreciable extent between the two excited states, *A*′ was fixed to its $^7B_2$ state value.

TABLE III. Rotational constants for $Mn^+(H_2O)$ ($cm^{-1}$).

| Constant | Ground state | $^7B_2$ state | $^7B_1$ state |
|---|---|---|---|
| $T_o$ | 0 | 30 210 | 32 267 |
| *A* | 13.81[a] | 12.8 ± 0.7 | 12.8[b] |
| *B* | 0.243[a] | 0.279 ± 0.05 | 0.277 ± 0.05 |
| *C* | 0.239[a] | 0.275 ± 0.05 | 0.273 ± 0.05 |
| $\varepsilon_{aa}$ | −3 ± 1 | 0.5 ± 0.5 | −4.2 ± 0.7 |

[a]Fixed to the calculated value.
[b]Fixed to the value in the $^7B_2$ state.

As seen above the spin-rotation parameter plays an important role in the simulations. The spin-rotation parameter $\varepsilon$ is determined by two factors.[41] For open-shell metal compounds, the dominant contribution is usually the second-order interaction between spin-orbit coupling and the Coriolis interaction. There is also some contribution from coupling of the electron spin to the magnetic field due to molecular rotation. Whitham and Jungen developed a pure precession model to predict the spin-rotation interaction in the p←s excited states of $CaNH_2$.[43] In this model, rotation about the *a* axis leads to mixing of the $p_x$ and $p_y$ orbitals, and hence of the $B_1$ and $B_2$ states. In addition to $CaNH_2$, it has been found to work quite well for $Mg^+(H_2O)$, $Ca^+(H_2O)$, and $Zn^+(H_2O)$. Solving for the resulting energies using perturbation theory, it predicts,[11]

$$\varepsilon_{aa} \approx \frac{4AA^{SO}\Lambda^2}{\Delta E}. \quad (6)$$

Here *A* is the rotational constant, $A^{SO}$ is the metal atom's effective spin-orbit interaction constant in the molecule (this is typically ∼85% of the value in the free atom), Λ = 1 for a $p_x$ or $p_y$ orbital, and ΔE is the energy difference between the $B_2$ and $B_1$ states.

In the ground states of $Mg^+(H_2O)$, $Ca^+(H_2O)$, and $Zn^+(H_2O)$ the only unpaired electron is in an s orbital, so the corresponding atomic states have no spin-orbit coupling, and Eq. (6) predicts $\varepsilon_{aa}'' = 0$. The measured spectra are consistent with this result.[6,13,44] These results are also verified by new simulations of the spectra of $Ca^+(H_2O)$ and $Zn^+(H_2O)$, with $\varepsilon_{aa}'' = \pm 1$ $cm^{-1}$ are nearly identical to those with $\varepsilon_{aa}'' = 0$. For $Mn^+(H_2O)$, $\varepsilon_{aa}''$ is initially set to zero because the $^7S_3$ ground state of $Mn^+$ has no spin-orbit coupling. However, simulations using $\varepsilon_{aa}'' = 0$ clearly do not reproduce the decreasing intensity to lower energy from 30 259 to 30 235 $cm^{-1}$ seen in Figure 5 (top) nor the decreasing intensity to higher energy starting at 32 300 $cm^{-1}$ as seen in Figure 5 (bottom). Instead, the simulations predict roughly constant intensity in these regions. In addition, the experimental $K_a' = 0 \leftarrow K_a'' = 1$ peaks are far too narrow for both states when compared to the simulations. Due to the $\varepsilon_{aa}K_a\Sigma$ energy term, septet $Mn^+(H_2O)$ (which has Σ = −3, −2, −1, 0, 1, 2, 3) is more sensitive to $\varepsilon_{aa}$ than doublet molecules, which have Σ = −1/2, +1/2. Simulations using $\varepsilon_{aa}'' = -3 \pm 1$ were best able to match the spectrum.

For $Mn^+(H_2O)$, the spin-orbit interaction constant for the $3d^5 4p$ states of $Mn^+$ is 62 $cm^{-1}$, so $A^{SO} \approx 53$ $cm^{-1}$, and $|\Delta E| = 2057$ $cm^{-1}$ (from the spectrum). This predicts $\varepsilon_{aa}' = \pm 1.3$ $cm^{-1}$ for the $^7B_2$ and $^7B_1$ states, respectively. While not in

quantitative agreement with the measured $\varepsilon_{aa}' = +0.5$ and $-4.2$ cm$^{-1}$ for the two states, it is qualitatively correct in predicting that the sign of $\varepsilon_{aa}'$ is different for the two states. The most distinctive sign of this is seen in the shapes of the $K_a' = 2 \leftarrow K_a'' = 1$ peak, which tails to the red in the $^7B_2$ state and to the blue in the $^7B_1$ state (Figure 5). The relatively poor performance of the pure precession model for $Mn^+(H_2O)$ is probably due to the small indirect spin-orbit contribution to $\varepsilon$ (the $Mn^+$ atomic spin-orbit coupling is substantially smaller than in $Ca^+$ and $Zn^+$), while the high spin of the manganese complex increases the contribution from direct interaction of the electron spin with the magnetic field due to molecular rotation.

The rotational structure in the electronic spectra of the $M^+(H_2O)$ complexes measured to date (M = Mg, Ca, Mn, Co, Ni, Zn) are all similar. Focusing on the transition metals, $Mn^+(H_2O)$ undergoes an allowed p←s transition, leading to a decrease in bond length, while the $Co^+(H_2O)$ and $Ni^+(H_2O)$ complexes undergo either d←d or s←d forbidden transitions, leading to greater repulsion and an increased bond length. Since rotational constants are strongly linked to the change in bond length, the *B* and *C* constants increase from the ground state to the excited state in $Mn^+(H_2O)$ and $Zn^+(H_2O)$, with the opposite occurring for the $Co^+(H_2O)$ and $Ni^+(H_2O)$ systems. Likewise the *A* constant decreases for the Mn and Zn complexes upon electronic excitation and decrease for the Ni and Co systems. Excited electronic states show varying lifetimes for these systems as indicated by observed Lorentzian linewidths ranging from 0.6 cm$^{-1}$ in $Ni^+(H_2O)$ to 6 cm$^{-1}$ in $Zn^+(H_2O)$. The spin-rotation constant $\varepsilon$ is zero in $Zn^+(H_2O)$, $-3$ cm$^{-1}$ in $Mn^+(H_2O)$, and significantly more negative for $Co^+(H_2O)$ and $Ni^+(H_2O)$ ($-6$ and $-12$ cm$^{-1}$, respectively). In the excited states, $\varepsilon$ can take positive or negative values, with the largest magnitude observed, 10 cm$^{-1}$, in $Zn^+(H_2O)$.

### C. Vibrational spectroscopy

Infrared spectroscopy studies are carried out to explore the effects of the metal on the O-H bonds in the complex's ground state and to try to provide direct measurement of the ground state $\varepsilon_{aa}''$ and $A''$ rotational constants without the involvement of the excited states. The vibrational spectrum of $Mn^+(H_2O)$ has been measured by Carnegie *et al.* via argon tagging.[17] Argon tagging, while expected to only affect the O-H stretching frequencies a small amount, completely changes the rotational structure. Vibrationally mediated photodissociation (VMP) is a tool which can be used to measure vibrational spectra of small, strongly bound ions without tagging. Our group has used VMP to measure the O−H stretching frequencies of $Ni^+(H_2O)$ and $Co^+(H_2O)$.[11,12] The simplest way to measure vibrational spectra using VMP is a depletion experiment. A laser operating in the visible or UV is set to an electronic transition which leads to photodissociation of ground state ions, while a second, IR, laser scans across the O-H stretching region. When the frequency of the IR laser corresponds to a vibrational transition, the ions are vibrationally excited. If these vibrationally excited molecules are no longer in resonance with the UV laser, this will lead to less photofragment signal.

Depletion scans were carried out for $Mn^+(H_2O)$, with the UV laser set to the $(v_3' = 1, K_a' = 0) \leftarrow K_a'' = 1$ transition at 30 655 cm$^{-1}$. A small amount of depletion (∼5%) was consistently seen at ∼3692 cm$^{-1}$ as shown in Figure S2 in the supplementary material.[45] Although the effect is small, it was reproduced in scans taken over several days. Setting the UV to other lines with $K_a'' = 1$ led to smaller depletion in this region. Unfortunately this was the only IR wavelength at which depletion was consistently observed, even after the UV laser was tuned to various transitions in the spectrum. The depletion experiment suffers from high background, which combines with shot to shot instability in the photofragment signal to give a noise level of ∼2%. In order to assign the transitions we correct the O-H symmetric and anti-symmetric stretch frequencies measured by Carnegie *et al.* for $Mn^+(H_2O)Ar$ ($\nu_1 = 3584$ cm$^{-1}$ and $\nu_5 = 3660$ cm$^{-1}$) with their calculated 2 cm$^{-1}$ shift for argon tagging to predict $\nu_1 = 3582$ cm$^{-1}$ and $\nu_5 = 3658$ cm$^{-1}$.[17] The VMP experiment monitors depletion from $K_a'' = 1$, so it is only sensitive to $K_a' = 1 \leftarrow K_a'' = 1$ for the symmetric stretch, which is a parallel band, and to $K_a' = 0,2 \leftarrow K_a'' = 1$ for the antisymmetric stretch, which is a perpendicular band. Simulations of the antisymmetric stretch using these frequencies and the ground state rotational constants in Table III predict absorption at 3652 and 3692 cm$^{-1}$. The observed depletion at 3692 cm$^{-1}$ thus clearly corresponds to $(v_5' = 1, K_a' = 2) \leftarrow (v_5'' = 0, K_a'' = 1)$, implying $\nu_5 = 3658$ cm$^{-1}$. Thus, binding to $Mn^+$ produces a 98 cm$^{-1}$ red shift in the O-H antisymmetric stretching frequency of water.

## IV. SUMMARY AND CONCLUSIONS

In summary, the electronic spectra of $Mn^+(H_2O)$ and $Mn^+(D_2O)$ were measured from 30 000 to 35 000 cm$^{-1}$ using photodissociation spectroscopy. The spectra show transitions to two excited electronic states, $^7B_2$ ($3d^5 4p_y$) and $^7B_1$ ($3d^5 4p_x$) with $T_0 = 30\,210$ and 32 274 cm$^{-1}$, respectively. The observed vibrations are assigned by comparing isotopic shifts between $Mn^+(H_2O)$ and $Mn^+(D_2O)$. These bands show long progressions in the Mn−O stretch with a frequency of ∼450 cm$^{-1}$ and partially resolved rotational structure. Combining the spectroscopic results with the guided ion beam measurement of the ground state zero Kelvin $Mn^+-H_2O$ dissociation energy (9900 ± 500 cm$^{-1}$)[4] gives binding energies of 18 200 ± 500 cm$^{-1}$ and 16 200 ± 500 cm$^{-1}$ for the $^7B_1(p_y)$ and $^7B_2(p_x)$ states, respectively. Electronic structure calculations at the CCSD(T)/aug-cc-pVTZ and TD-DFT B3LYP/6-311++G(3df,3pd) predict $Mn^+$-$H_2O$ bond lengths in the excited states that are in excellent agreement with experimental results. Progressions in the in-plane and out-of-plane bends are also observed in the $^7B_2$ and $^7B_1$ state, respectively. The observed rotational contours are fit to give spin-rotation constants $\varepsilon_{aa}'' = -3 \pm 1$ cm$^{-1}$ for the ground state and $\varepsilon_{aa}' = 0.5 \pm 0.5$ cm$^{-1}$ and $\varepsilon_{aa}' = -4.2 \pm 0.7$ cm$^{-1}$ for the $^7B_2$ and $^7B_1$ excited states of $Mn^+(H_2O)$, respectively, and an $A'$ rotational constant of 12.8 ± 0.7 cm$^{-1}$ for the $^7B_2$ state. Vibrationally mediated photodissociation studies determined the O-H

antisymmetric stretching frequency in the ground electronic state to be 3658 $cm^{-1}$. Overall the excited states of $Mn^+$ interact more strongly with water than the ground state, resulting in decreased Mn-O bond length in the excited states, and an increase in the H-O-H angle.

## ACKNOWLEDGMENTS

Financial support from the National Science Foundation under award CHE-1300501 is gratefully acknowledged.

[1]M. K. Beyer, Mass Spectrom. Rev. **26**, 517–541 (2007).
[2]T. F. Magnera, D. E. David, and J. Michl, J. Am. Chem. Soc. **111**, 4100–4101 (1989).
[3]P. J. Marinelli and R. R. Squires, J. Am. Chem. Soc. **111**, 4101–4103 (1989).
[4]N. F. Dalleska, K. Honma, L. S. Sunderlin, and P. B. Armentrout, J. Am. Chem. Soc. **116**, 3519–3528 (1994).
[5]F. Misaizu, M. Sanekata, K. Tsukamoto, K. Fuke, and S. Iwata, J. Phys. Chem. **96**, 8259–8264 (1992).
[6]C. T. Scurlock, S. H. Pullins, J. E. Reddic, and M. A. Duncan, J. Chem. Phys. **104**, 4591–4599 (1996).
[7]H. Ishikawa, T. Nakano, T. Eguchi, T. Shibukawa, and K. Fuke, Chem. Phys. Lett. **514**, 234–238 (2011).
[8]S. G. Donnelly, C. A. Schmuttenmaer, J. Qian, and J. M. Farrar, J. Chem. Soc., Faraday Trans. **89**, 1457–1465 (1993).
[9]D. E. Lessen, R. L. Asher, and P. J. Brucat, J. Chem. Phys. **93**, 6102–6103 (1990).
[10]B. Scharfschwerdt, C. van der Linde, O. P. Balaj, I. Herber, D. Schutze, and M. K. Beyer, Low Temp. Phys. **38**, 717–722 (2012).
[11]J. S. Daluz, A. Kocak, and R. B. Metz, J. Phys. Chem. A **116**, 1344–1352 (2012).
[12]A. Kocak, G. Austein-Miller, W. L. Pearson III, G. Altinay, and R. B. Metz, J. Phys. Chem. A **117**, 1254–1264 (2013).
[13]Y. Abate and P. D. Kleiber, J. Chem. Phys. **122**, 084305 (2005).
[14]P. D. Carnegie, B. Bandyopadhyay, and M. A. Duncan, J. Chem. Phys. **134**, 014302 (2011).
[15]N. R. Walker, R. S. Walters, E. D. Pillai, and M. A. Duncan, J. Chem. Phys. **119**, 10471–10474 (2003).
[16]P. D. Carnegie, B. Bandyopadhyay, and M. A. Duncan, J. Phys. Chem. A **112**, 6237–6243 (2008).
[17]P. D. Carnegie, B. Bandyopadhyay, and M. A. Duncan, J. Phys. Chem. A **115**, 7602–7609 (2011).
[18]R. S. Walters and M. A. Duncan, Aust. J. Chem. **57**, 1145–1148 (2004).
[19]R. S. Walters, E. D. Pillai, and M. A. Duncan, J. Am. Chem. Soc. **127**, 16599–16610 (2005).
[20]P. D. Carnegie, A. B. McCoy, and M. A. Duncan, J. Phys. Chem. A **113**, 4849–4854 (2009).
[21]B. Bandyopadhyay, K. N. Reishus, and M. A. Duncan, J. Phys. Chem. A **117**, 7794–7803 (2013).
[22]B. Bandyopadhyay and M. A. Duncan, Chem. Phys. Lett. **530**, 10–15 (2012).
[23]J. Sasaki, K. Ohashi, K. Inoue, T. Imamura, K. Judai, N. Nishi, and H. Sekiya, Chem. Phys. Lett. **474**, 36–40 (2009).
[24]K. Furukawa, K. Ohashi, N. Koga, T. Imamura, K. Judai, N. Nishi, and H. Sekiya, Chem. Phys. Lett. **508**, 202–206 (2011).
[25]T. Iino, K. Ohashi, K. Inoue, K. Judai, N. Nishi, and H. Sekiya, J. Chem. Phys. **126**, 194302 (2007).
[26]Y. Z. Li, G. J. Wang, C. X. Wang, and M. F. Zhou, J. Phys. Chem. A **116**, 10793–10801 (2012).
[27]C. van der Linde and M. K. Beyer, J. Phys. Chem. A **116**, 10676–10682 (2012).
[28]J. T. O'Brien and E. R. Williams, J. Phys. Chem. A **115**, 14612–14619 (2011).
[29]M. Rosi and C. W. Bauschlicher, Jr., J. Chem. Phys. **90**, 7264–7272 (1989).
[30]M. Trachtman, G. D. Markham, J. P. Glusker, P. George, and C. W. Bock, Inorg. Chem. **37**, 4421–4431 (1998).
[31]A. Irigoras, J. E. Fowler, and J. M. Ugalde, J. Am. Chem. Soc. **121**, 8549–8558 (1999).
[32]J. Husband, F. Aguirre, P. Ferguson, and R. B. Metz, J. Chem. Phys. **111**, 1433 (1999).
[33]R. B. Metz, Adv. Chem. Phys. **138**, 331–373 (2008).
[34]X. Zhu, A. H. Nur, and P. Misra, J. Quant. Spectrosc. Rad. Trans. **52**, 167–177 (1994).
[35]M. Citir, G. Altinay, G. Austein-Miller, and R. B. Metz, J. Phys. Chem. A **114**, 11322–11329 (2010).
[36]M. J. Frisch, G. W. Trucks, H. B. Schlegel *et al.*, Gaussian 09, Revision D.01, Gaussian, Inc., Wallingford, CT, Pittsburgh, PA, 2010).
[37]K. F. Willey, C. S. Yeh, D. L. Robbins, J. S. Pilgrim, and M. A. Duncan, J. Chem. Phys. **97**, 8886–8895 (1992).
[38]A. Kramida, Y. Ralchenko, J. Reader, and NIST ASD Team, NIST Atomic Spectra Database (ver. 5.2) (National Institute of Standards and Technology, Gaithersburg, MD, 2014).
[39]J. D. Mosley, T. C. Cheng, S. D. Hasbrouck, A. M. Ricks, and M. A. Duncan, J. Chem. Phys. **135**, 104309–104306 (2011).
[40]H. M. Pickett, J. Mol. Spectrosc. **148**, 371–377 (1991).
[41]G. Tarczay, S. Gopalakrishnan, and T. A. Miller, J. Mol. Spectrosc. **220**, 276–290 (2003).
[42]J. M. Brown and T. J. Sears, J. Mol. Spectrosc. **75**, 111–133 (1979).
[43]C. J. Whitham and C. Jungen, J. Chem. Phys. **93**, 1001–1008 (1990).
[44]H. Watanabe, S. Iwata, K. Hashimoto, F. Misaizu, and K. Fuke, J. Am. Chem. Soc. **117**, 755–763 (1995).
[45]See supplementary material at http://dx.doi.org/10.1063/1.4901982 for MO diagram showing the 3*d*, 4*s*, and 4*p* orbitals in $Mn^+(H_2O)$ (Figure S1) and VMP depletion scan and simulation (Figure S2).